https://doi.org/10.1016/j.jhazmat.2019.121208

Spatial distribution and molecular speciation of copper in indigenous plants from contaminated mine sites: Implication for phytostabilization

Jin-li Cui[1, 2], Yan-ping Zhao[1], Ting-shan Chan[3], Li-li Zhang[4], Daniel C.W. Tsang[1], Xiang-dong Li[1*]

[1]*Department of Civil and Environmental Engineering, The Hong Kong Polytechnic University, Hung Hom, Kowloon, Hong Kong*

[2]*Key Laboratory for Water Quality and Conservation of the Pearl River Delta, Ministry of Education; School of Environmental Science and Engineering, Guangzhou University, Guangzhou, China*

[3]*National Synchrotron Radiation Research Center, 101 Hsin-Ann Road, Hsinchu Science Park, Hsinchu 30076, Taiwan*

[4]*Shanghai Synchrotron Radiation Facility, Shanghai Institute of Applied Physics, Chinese Academy of Sciences, Shanghai 201214, China*

Corresponding author (X.D. Li): E-mail address: cexdli@polyu.edu.hk; Fax: +852-2334-6389; Tel.: +852-2766-6041.

Abstract

Contaminated mining sites require ecological restoration work, of which phytoremediation using appropriate plant species is an attractive option. Our present study is focused on one typical contaminated mine site with indigenous plant cover. The X-ray absorption near edge structure (XANES) analysis indicated that Cu (the major contaminant) was primarily associated with goethite (adsorbed fraction), with a small amount of Cu oxalate-like species (organic fraction) in mine affected soil. With

growth of plant species like *Miscanthus floridulus* and *Stenoloma chusanum*, the Cu-oxalate like organic species in rhizosphere soil significantly increased, with corresponding decrease in Cu-goethite. In the root cross-section of *Miscanthus floridulus*, synchrotron-based micro-X-ray fluorescence (μ-XRF) microscopy and X-ray absorption near edge structure (XANES) indicated that most Cu was sequestered around the root surface/epidermis, primarily forming Cu alginate-like species as a Cu-tolerance mechanism. From the root epidermis to the cortex and vascular bundle, more Cu(I)-glutathione was observed, suggesting reductive detoxification ability of Cu(II) to Cu(I) during the transport of Cu in the root. The observation of Cu-histidine in root internal cell layers showed another Cu detoxification pathway based on coordinating amino ligands. *Miscanthus floridulus* showed ability to accumulate phosphorous and nitrogen nutrients in rhizosphere and may be an option for *in situ* phytostabilization of heavy metals in contaminated mining area.

Keywords: Contaminated sites; Metal uptake; Phytostabilization; Synchrotron-based X-ray techniques; Rhizosphere; Copper

Introduction

In the last hundred years, surface soil in many parts of the world has been contaminated by large amounts of mine tailings or wastewater generated from mining activities [1, 2]. The resulting high levels of trace metals, including Cu, Zn, and Pb, may a pose severe risk to the nearby soil, wildlife, agricultural field, and even human beings [1, 3, 4]. Once a soil system is contaminated by human activities, the affected ecosystem can be difficult to remediate and restore [5-7]. The indigenous plants are adapted to the mine soil with high concentrations of metal contaminants and a low level of available nutrients [8-10]. These plant species enduring severe conditions may be used in green remediation technology (*e.g.,* phytomanagement or phytoremediation), which are usually sustainable and relatively inexpensive and have been demonstrated as effective for *in situ* ecorestoration of mine-polluted soil in previous studies [5, 8, 11, 12].

Phytoremediation efficiency relies on the understanding of the efficient uptake and transformation/stabilization of trace metals by plant roots [11, 13, 14]. Among trace metals, Cu is an essential micronutrient and plays a vital role in the normal growth of plant; however, Cu can have a highly toxic effect at high concentrations. The absorbed Cu is usually accumulated in the cell wall and vacuoles, binding with O-rich ligands in hyperaccumulator plants [14]. In non-hyperaccumulators, Cu is usually bound with strong HS-ligands such as metallothionein or phytochelatin in roots as a detoxification mechanism [13, 15]. Furthermore, reduction from Cu(II) to Cu(I) during plant uptake may occur and play a fundamental role in Cu detoxification in non-hyperaccumulators. However, detailed information for Cu reduction process from soil rhizosphere to plant is very limited and remains largely unclear. For example, Cu(II) may be absorbed by bamboo roots before reduction, as only Cu(II) was observed in roots [16]. On the other hand, the reduction of Cu(II) before absorption probably occurs in root cell during uptake by rice, as evidenced by the slightly lighter Cu isotopes [17, 18]. Further *in situ* evidence on Cu transformation process in the soil-plant root system is urgently needed for understanding Cu uptake and detoxification, which is very important for phytoremediation at contaminated sites.

In situ distribution/transformation of Cu within plant roots has been recently investigated, and the results provided valuable information on both the oxidation state and spatial distribution [18, 19]. Possible reduction of Cu(II) to Cu(I) during root absorption was suggested because Cu(I) was observed in plant root, such as oat root [18], rice root [19], and ryegrass root [13] using bulk X-ray absorption near edge structure (XANES) spectroscopy, in agreement with Cu isotopic fractionation results [17, 18]. However, those previous studies only focused on Cu valence state in root in hydroponics experiments, which may be different from real plant species under field soil conditions. Furthermore, the exact location of the different Cu species remains unclear from rhizosphere soil to root surface, and among internal micro-region of the root cross-section. Therefore, the present research focused on the critical rhizosphere processes from a mine-impacted field site, including the micro-spatial distribution, molecular speciation, and transport of Cu from bulk soil (non-rhizosphere) to

rhizosphere soil, and plant root parts (*e.g.,* root surface to root internal cell layers).

By investigating the indigenous wild plant species and their niches from a typical mine site of Dabaoshan in China, we intend to elucidate how Cu can be absorbed and transformed by plant from contaminated soil. The *in situ* spatial distribution and molecular speciation of Cu in root cross sections were studied using micro-X-ray fluorescence (μ-XRF) microscopy and μ-XANES. The results will improve the potential application of wild plant species in ecological restoration work [8].

Materials and methods

Sample site, collection, and treatment

The Dabaoshan Mine (24°31′28″N, 113°43′42″E) is the largest polymetallic sulfide deposit and located in Shaoguan, Guangdong Province, and has been in full-scale mining operation for iron ores and Cu since the 1960s, and large scale contaminated sites require much ecological restoration work [2, 8]. During the field survey and sampling, two kinds of wild plant species including *Miscanthus floridulus* and *Stenoloma chusanum* were widely observed in the mining area, consistent with previous reports [20, 21], and were employed as the representative indigenous plants to study the rhizosphere processes of Cu and subsequent plant uptake behavior. Rhizosphere soil attached to plant roots was carefully collected using a clean brush into a small plastic bag after removing the soil particles loosely adhering to the roots by gently hand-shaking [22], and the respective non-rhizosphere bulk soil was also collected at least 10 cm away from the plant root. Underground mining waste samples without any erosion or irrigation were also collected at the sampling site. The samples were transported in a cooler box and stored at 4 °C once arriving at the laboratory. Plant samples were washed with tap water and deionized water three times to remove the extraneous soil particles, dried at 80 °C for 3 days, and ground before analysis. Some fresh plant and soil samples were stored at 4 °C and prepared for further synchrotron characterization.

Sample analysis

Soil pH was determined using a Model 225 meter (Denver Instrument, USA) by stirring air-dried <10-mesh-sieved (2-mm) soil in deionized water (1/2.5, g/mL) for 30 min on an end-over-end rotator. The available phosphorous (P) and TOC (TOC analyzer, Shimadzu) were determined in the extract by reacting 4 ºC-stored soils with $CaCl_2$ (0.01 M) solution (1/10, g/mL) for 2 hours. The P concentration in the centrifuged suspension was determined using the molybdenum blue spectrophotometric method at 880 nm using an UV-Vis spectrophotometer (SPECTRA UV-11, MRC, Germany). Bioavailable nitrate and ammonium were determined by mixing soils (4 ºC stored, within 24 hours) with KCl (2.0 M) solution (1/12, g/mL) for one hour with Nessler's reagent using a spectrophotometer (DR 3900, Hach Co., USA) [23].

Plant available trace/major metals in soil were determined in the filtrated (0.45-μm) suspension from mixing air-dried (2-mm) soil with 0.01 M $CaCl_2$ (1/10, g/mL) for 120 min. The samples were digested with 4:1 (V/V) concentrated HNO_3 and $HClO_4$ [24]. Metal elements including Cu, Ca, Mg, Fe, and Al were analyzed using ICP-OES (Agilent, 700 Series) and ICP-MS (Agilent, 7700 Series) and reported on a dry weight basis. The influence of plant rhizosphere on soil parameters and available trace metals distribution were analyzed using paired-sample t-test in SPSS software version 22.0.

Samples characterization

The fresh *M. floridulus* root samples were washed with tap water, rinsed in deionized water, embedded in Tissue-Tech (Sakura Finetek, Japan), and cut into cross-sections of ~50-μm using a stainless steel blade at -20 ºC in a cryotome (Cryostat CM1950, Leica Microsystems, Nussloch, Germany) [4, 25]. The transversal section was sealed between two layers of Kapton tape, freeze-dried, and analyzed using μ-XRF and μ-XANES at beamline 15U at the Shanghai Synchrotron Radiation Facility (SSRF), China [26, 27]. The μ-XRF analysis was conducted with the monochromator set at 12000 eV, a 50 × 50 μm beam, a dwell time of three seconds per pixel, and a step size of 50 μm. The peak intensities for Cu, Fe, Al, S, P, Ca, and K were collected at each pixel and then imaged for elemental distribution using Igor Pro 5.0. Cu K-edge μ-

XANES spectra for the interested points (IS) were collected.

The -20 ℃ stored rhizosphere and non-rhizosphere soil samples were analyzed using XANES at Cu K-edge (8979 eV) at beamline 01C1, and Fe K-edge (7112 eV) at beamline BL16A1 at the National Synchrotron Radiation Research Center (NSRRC) in Taiwan. Inorganic Cu standards included $CuSO_4$, $CuCO_3$, $Cu(OH)_2$, $Cu_3(PO_4)_2$, CuS, CuO, Cu-goethite, and CuCl as solid phase. The complexes of organic Cu standards included Cu-oxalate (carboxylate bidentate complex, representing soil organic substance), Cu-alginate (carboxylate complex, representing polysaccharides-like cell wall structure), Cu-histidine (amino/carboxylate complex), and thiol-S ligand-bound Cu(I) (Cu(I)-glutathione and Cu(I)-cysteine) and were prepared as solution standards in the beamline station [13, 28]. Replicate analysis of one sample indicated no obvious transformation of Cu species caused by the X-ray beam during XANES collection (Figure S1). Iron standard references in the present study included ferrihydrite, goethite, akaganeite, lepidocrocite, hematite, magnetite, and pyrite. Metal foils of Cu and Fe were used to calibrate the absorption energy. Spectra of solid standards were acquired in transmission mode, while solution standard references, plants, and soil were acquired in fluorescence mode with a Lytle detector. Because the spectra of Cu XANES and μ-XANES were collected at two beamlines from SSRF and NSRRC, the E_0 values were carefully aligned according to the metal foil and the same standard references. The selection of standard references for linear combination fit (LCF) analysis was tested by principal component analysis (Table S1) and target transformation testing (Table S2) in the SIX-PACK code [13, 29, 30]. The XANES analysis using linear combination fit was performed with the Athena program in the IFEFFIT computer package [31]. More analysis details can be found in our previous studies [13, 32].

2.5 QA/QC

In the analysis of metals, standard reference material (NIST SRM 2711a & 1573a, USA) was used for every batch of digestion and analysis. Reagent blank and analytical triplicates, comprising 10% of the total samples, were also used to test the accuracy and

precision. The digestion recovery rates for the reference materials were approximately 91.7 ± 9.9% for Cu, 48.6 ± 0.6% for Fe, 38.7 ± 0.4% for Al, and 58.2 ± 0.9% for Mn, and the relatively lower recovery rates of Fe, Al, and Mn were due to incomplete dissolution of alumina-silicates with HNO_3 and $HClO_4$. Triplicates of random samples were analyzed with standard errors <10% for all the samples.

Results

Characterization of the mine soil

Soil parameters including pH, TOC, P, nitrate and ammonia (Table 1) often show important influence on the plant bioavailable metals and vegetation condition. The pH in the mine soil after deionized water extraction ranged from 3.48 to 4.56 (Table 1). The available nutrients for plant including organic matter, P, nitrate, and ammonium in the soil were analyzed after $CaCl_2$ extraction (Table 1), which reflect the adaptation of plants to adverse soil conditions [33]. After extraction, the surface mine soil with some vegetation had 2.3-4.6 fold higher TOC values in comparison with non-vegetated mine soil. Furthermore, TOC values in rhizosphere soil were 1.8-2.6 times higher than in the non-rhizosphere soil. The rhizosphere soil contained 0.18-0.20 mg/L P in the extract, higher than non-rhizosphere soil, at 0.14-0.16 mg/L. Consistently, 2.51-5.20 mg/L nitrate and 0.06-0.16 mg/L ammonia were observed in the rhizosphere soil extract, higher than the non-rhizosphere soil with 0.30-1.06 mg/L nitrate and 0.01-0.03 mg/L ammonia, respectively.

The analyzed soil geochemical parameters showed significant difference (p=0.101) in rhizosphere soil in comparison with non-rhizosphere soil for *M. floridulus*. However, no significant difference (p=0.003) was observed for *S. chusana*. Even though the correlation analysis cannot necessarily reflect the cause-effect relationship, the comparison results suggested that *M. floridulus* may show higher ability to change the soil physiochemical properties in rhizosphere than *S. chusana*.

Copper and major metals in soil and plant samples

Total Cu concentrations in rhizosphere and non-rhizosphere samples showed similar levels (Table 2). Nevertheless, the extraction results (Table 1) indicated a significantly higher concentration of available Cu in the rhizosphere soil (0.08-1.34 mg/L) than in the non-rhizosphere soil (0.06-1.02 mg/L) (p<0.01). Compared to the un-vegetative mine waste containing 0.06 mg/L available Cu, relatively higher available concentrations of Cu were observed after plant growth in the mine soil, such as the highest available Cu in the rhizosphere soil from *M. floridulus* with the lowest pH value (3.48). The results indicate that Cu becomes relatively more mobilized after plant growth probably caused by the organic exudates and its influence on lowing pH [33-35].

For the two plant species, Cu showed high concentrations in roots with 264-535 mg-Cu/kg and relatively low contents in shoots (20-29 mg-Cu/kg) (Table 2). Of the two species, the *Miscanthus* genus, showed strong vitality with high biomass yield in various harsh environments around the world [36]. The bioaccumulation factor (BCF) and translocation factor (TF) values of the analyzed metals for the studied plant species were calculated shown in Table 2. All of the BCF and TF values besides Mn were less than 1, showing no Cu hyperaccumulation ability of the selected plant species. Even though many engineering plants show higher BCF and TF values than 1, the current plant species were tolerant to high concentrations of Cu in soil and can reduce the bioavailable fractions of Cu by sequestration in the rhizosphere regions, and may be useful for phytostabilization [37]. The uptake process of Cu was investigated in detail below.

For the major elements, much higher concentrations of Fe (168-210 g/kg) and Al (106-109 g/kg) were observed in the mine soils compared to Mn (0.45-1.30 g/kg) (Table 2). In the aerobic soils, Fe/Al/Mn occurs predominately in the form of highly insoluble oxy(hydr)oxides that are largely unavailable to plants. $CaCl_2$ extraction of the soil

samples (Table 1) showed relatively low levels of available Fe (0.01-0.32 mg/L), Al (0.10-9.88 mg/L), and Mn (ND-3.90 mg/L). Much higher concentration of Fe (2850-8050 mg/kg in roots and 204-498 mg/kg in shoots) and Al (870-8000 mg/kg in roots and 203-357 mg/kg in shoots) was observed in plants (Table 2) compared to Mn (0.5-2.5 mg/kg in roots and 2.6-11.7 mg/kg in shoots), probably due to the large pool of Fe and Al in mine soil. High concentrations of Fe were usually reported in plant root and shoot samples in previous studies because Fe acts an essential nutrient element for plant culture [38, 39]. Abundant Al may be toxic for plant growth [40], and the collected wild plants were tolerant to high Al, consistent with previous studies of elevated Al concentration in plants, such as 2099-7100 mg/kg in roots [22, 41, 42] and 51-5733 mg/kg in shoots [43, 44].

Spatial distribution of Cu and other elements in root section

To elucidate the Cu uptake mechanism by plants from soil, representative root samples of *M. floridulus* from the mining area were analyzed using μ-XRF (Figure 1) and μ-XANES (Figure 2). The relative comparison of the intensities between each element in the pixels from the μ-XRF map can help identify their spatial distribution [45].

The μ-XRF mapping results showed that most of the absorbed Cu in plants was retained as a layer around the root surface of rhizodermis and outer cortex for *M. floridulus* (Figure 1). Relatively higher concentrations of Cu were observed in the root epidermis region across the root section. The distribution of Cu around the root section for *M. floridulus* was consistent with a high abundance of Fe and other elements, showing a significant linear correlation ($R \geq 0.817$ with $p < 0.01$) of Cu with Fe, Al, Mn, and other nutrient elements such as K, Ca, P, and S (Figure S2). The observation of a higher Fe content on the root surface and epidermis than in the internal areas including the cortex and xylem is consistent with previous studies in both aerobic and anaerobic flooding conditions [46-48]. Although a much high amount of Cu was sequestered on

the root surface, Cu was still translocated into the xylem, as shown by several hot spots of Cu in the samples (Figure 1).

Molecular speciation of Cu from soil to plant

The spectral features of Cu K-edge XANES are sensitive to its molecular coordination in the environment [16, 49], and can be used to investigate the molecular speciation change of Cu from the soil to the root surface and root intersection (Figure 2). The main peak at (a) (Figure 2-I) was probably due to the 1s to 4p main edge transitions contributable to the Cu(II) species in the samples, mostly higher than 8985 eV [50]. The pre-edge peaks (b) (i.e., 8982 eV for Cu-glutathione and 8985 eV for Cu(I)Cl) reflect the presence of Cu(I) species in the samples, which correspond to the transitions of 1s-4p_{xy} [16].

The Cu K-edge XANES analysis of the soil samples (Figure 2) showed a primary peak at approximately ~8976 eV, indicating the dominance of Cu(II). The LCF analysis (Table 3) exhibited that in the original mine soil, Cu was primarily associated with the adsorbed species on goethite (72%), with some amount of CuS (12%) and Cu-oxalate (16%). After natural weathering/erosion and plant growth, the oxalate-associated Cu fraction (31-80%, Table 3) increased in the soils, coupled to the decrease in the adsorbed Cu species on goethite, suggesting the greater bonding affinity of organic matter to Cu [51, 52]. Specifically, for the non-rhizosphere soil, Cu was primarily associated with Fe oxides (42-69%) and Cu-oxalate (31-55%). While in the rhizosphere soil samples, Cu was associated with Fe oxides (20-55%) and Cu-oxalate (41-80%). No Cu(I) was found in the rhizosphere and non-rhizosphere soil because no significant peak was observed for Cu(I)-glutathione or Cu(I)Cl (Figure 2). The observed much high percentage of goethite (51-95%) as Fe phase in the soil samples (Figure 3 and Table S3) contributed to the large amount of adsorbed Cu species.

After absorption of Cu on the root surface, Cu was mostly bound to alginate (65-100%, Table 3). The adsorbed Cu(II) species (by goethite) was not observed in the root surface from the root section, inconsistent with the large amount of Fe on the root

surface, suggesting that the Fe plaque on the root surface was not a dominant Cu sequestrator for *M. floridulus* in this study.

From the root surface to the stele of *M. floridulus*, a clear changing shift in Cu species was observed. Cu(I) gradually increased, as identified by the increasing magnitude of the pre-edge peak at ~8984 eV of Cu(I)-glutathione/cysteine (Figure 2). The four interested spots (IS 1-4) in the root intersection consisted of three primary Cu species including Cu-alginate, thiol-S bound Cu(I), and Cu-histidine (Table 3). Alginate acid-associated Cu decreased gradually from the epidermis to the xylem (from 92% to 45%), and thiol-S bound Cu(I) (i.e., Cu(I)-glutathione and Cu(I)-cysteine) gradually increased (from 8 to 27%), with some amount of Cu-histidine (27% for IS4) formed in the xylem.

Discussion

Distribution and mobility of Cu from mine soil to plant root

The Cu distribution difference in root cross sections possibly resulted from different Cu concentration/species exposure, exposure duration, Cu contents in plant, and plant species. The high concentration of Cu and Fe around the root epidermis rather than in the vascular tissue is consistent with a previous report from an urban wetland brownfield site [39]. The uptake of Fe by plant often generates Fe plaques on the root surface by Fe(II) oxidation induced in the rhizosphere [48, 53]. Trace metals are often sequestered by Fe plaques around roots from both arid and paddy soils, and their translocation is thereafter inhibited from the root surface/epidermis to the root endodermis/cortex [39, 54]. Nevertheless, the interaction between Cu and Fe cannot be exactly determined by spatial distribution analysis only, as the rhizosphere niche is very complicated. Other studies also indicated that Fe plaques showed no promotion effect on the uptake of trace metals from soils to plants [55, 56]. The reason for the contrary effect of Fe plaques on trace metals probably relies on the root exudates, trace metal and Fe bioavailability, soil chemistry characteristics such as like pH and redox potential, and root anatomy of various plant species [57-59].

306 In mining site, XANES analysis indicated Cu(II) as the dominant valence state,
307 with the primary fraction as the Fe oxide-adsorbed species (Figure 2), consistent with
308 a previous study that very low amount of organic matters associated Cu species (0.55%)
309 exists [60]. The consistent results indicated that most of the Cu was retained on
310 abundant Fe oxides in the original mine soil, and the species is not easily absorbed by
311 plants, unlike the aqueous Cu species usually used in hydroponic/pot experiments.
312 After plant vegetation, the Cu fraction is transformed from adsorbed species to Cu-
313 oxalate in the rhizosphere soil, which should be caused by the high number of organic
314 exudates identified by the high TOC value in the soil extract (Table 1). Complexation
315 of metals by the secreted organic exudates in the rhizosphere is one of the primary plant
316 defence strategies [61].

317 The accumulation of toxic metals within the cell wall on root epidermis usually
318 plays a critical role in plant detoxification [61, 62], particularly under toxic stress with
319 high concentrations. The observation of an extremely high concentration of Cu in the
320 root epidermis region across the root section is consistent with previous reports for
321 *Phragmites australis* from an urban brownfield site [39], bamboo (exposing 100 mM
322 Cu plus 1.1 mM Si in hydroponic conditions for 70 days) [16], and cowpea (exposing
323 1.5 μM Cu in hydroponic conditions for 24 hours) [63]. From the image in Figure 1-g,
324 some compartments of the root surface/epidermis were much thicker, where the cell
325 walls synthesize more phytochelators to sequester heavy metals and limit their
326 absorption/translocation [64, 65]. Therefore, the indigenous plant species *M. floridulus*
327 showed high tolerance and low translocation of Cu, which also explained the tolerance
328 capacity for Cd by the same genus, in *M. sacchariflorus* [36].

329 A recent study indicated that Cu was concentrated in the vascular bundles (possibly
330 in the xylem tissue) rather than on the epidermis and cortex in *Oryza sativa* (50 μM Cu
331 for 7 days) [19] and the Cu-tolerant plant *Commelina communis* (100 μM for 15 days)
332 [66], rather than in the rhizodermis or the outer cortex. In other studies, the molecular
333 species of Cu sequestered in the root epidermis and root xylem was studied to
334 understand the uptake and translocation of Cu [67, 68]. The XANES analysis showed

a high proportion of Cu-alginate in the root, indicating that the plant sequesters most of the Cu within the cell wall components, consistent with the large portion of the Cu-cell wall structure (79%) in rice roots [19]. The alginate ligand represents a type of natural polysaccharide with multiple hydroxyl groups on root cell walls [69, 70], and often binds absorbed heavy metals, including Cu, Zn, and Pb. Therefore, the alginate structure in *M. floridulus* roots inhibits the excess entrance of heavy metals to the root vascular tissues for translocation as the first defence strategy, and therefore reduces Cu toxicity [62, 70, 71]. For the high Cu concentration (264 mg/kg) in *M. floridulus*, as the primary protective barrier, the root epidermis sequestered most of the Cu by the abundant alginate-like structure.

Molecular species of Cu in root transversal sections

The transformation of Cu species from root surface to root xylem in the root section reflects the fate of Cu from absorption to detoxification metabolism. The Cu(I)-glutathione complex represents the reduced thiol Cu(I) species from the detoxification product of Cu(II) by a thiol-ligand in plant [28]. The general interactions of thiol HS-containing ligands with Cu reduce the bioavailability of Cu and thereby avoid possible toxicity and damage to plants [16, 72]. The observed organic complex of Cu-histidine and thiol-S bound Cu(I) in the root vascular tissues may be the Cu form transported to the aerial part *M. floridulus* [13, 18]. On the other hand, Cu-histidine in IS-4 may be the sequestered Cu form on the cell wall of the vascular bundle for plant detoxification of the excess absorbed Cu [68]. More histidine produced in plant root can form complexes with Cu with a high association constant [73].

The uptake and transformation of Cu by plants is complex, depending on plant species, Cu levels and chemical species, and environmental conditions [62, 74]. In the root surface, most of the Cu was identified as Cu-alginate (82% for IS-1 and 92% for IS-2, Figures 1 and 2), indicating that most of the absorbed Cu is in the form of Cu(II). Similarly, for bamboo, a monocot non-hyperaccumulator, only Cu(II) binding to amino and carboxyl ligands was observed in the root [16]. The uptake of Cu(II) should be majorly contributed by the symplastic pathway under these high concentration of

available Cu (1.34±0.06 mg/L), given that the negative charged cell wall is the primary site of apoplastic binding and transport [61]. Nevertheless, the apoplastic symplastic pathway for Cu(II) uptake cannot be neglected because Cu(II) can be absorbed by the root from soil solution probably via unspecific iron-regulated transporter (IRT)-like protein (ZIP) family [75] or the Fe-phytosiderophore yellow stripe 1-like (YSL) transporter [76, 77].

The observation of thiol-S bound Cu(I) on the root surface/epidermis (17% for IS-1, Figures 1 and 2) suggested that Cu(II) might be reduced within the plant root epidermis layer. A recent study observed Cu(I) in isolated border cells from the rice root tip under hydroponic culture [78]. Previous results have also observed Cu(I) in monocot plant root samples such oat root (77-88%) [18], rice root (5%) [19], and ryegrass root (20%) [13] using the bulk-XAS technique, although no exact location of Cu(I) was reported from the root cross-sections. Moreover, a reduction process before absorption may occur at the root cell wall during uptake as evidenced by the lighter Cu isotopes in rice [17] and oat [18], although many processes resulted in comparatively small fractionation. From the plant physiology studies for monocot rice [79], the related Cu transporter COPT/Ctr-like protein family was reported, which mediated the acquisition of Cu(I) in roots [74]. Therefore, solid evidence of Cu(I) with thiol-like ligands was first observed in the monocot species *M. floridulus*, which may reduce Cu(II) to Cu(I) on the root epidermis, probably by a specific Cu reductase (possibly FRO4/5) and absorb the reduced Cu(I) via COPT1 [80].

For the cortex and xylem of roots, more thiol-S bound Cu(I) (IS3 with 24% and IS4 with 27%, Figures 1 and 2) was observed than the root surface compared with the rhizodermis region. The reduction process from Cu(II) to Cu(I) in the root is consistent with the detoxification of Cu(II), which often occurs in the cytoplasm and stored as a Cu(I) complex with thiol-bearing ligands [18]. In the non-hyperaccumulators, Cu was usually bound with strong S ligands such as metallothionein or phytochelatin as a detoxification process [15], which is very similar to *M. floridulus* in this study.

Uptake and transformation of Cu by plants from contaminated mine areas

Based on our analysis and previous studies, an uptake scheme (Figure 4) for Cu can be drawn for the indigenous plant (*M. floridulus*) at a real contaminated site. Copper is firstly solubilized from the immobile fraction like adsorbed fractions on iron oxide into the soil solution facilitated by various organic exudates excreted by the plant (Figure S3 A&B). Once the available Cu is taken up by the roots as nutrients, most Cu is sequestered on the rhizodermis and outer cortex complexed with alginate acid-like components, which increases the tolerance of the indigenous plants and limits Cu translocation from roots to shoots.

During the plant uptake process, two pathways may exist. On one hand, Cu(II) can be absorbed via the apoplastic route (Figure 4-I) or the symplastic pathway (Figure 4-II) probably via the YSL or ZIP membrane transporters [74-76], in which Cu(II) is directly absorbed without reduction. On the other hand, some Cu(II) is first reduced to Cu(I) on the root surface (Figure 4-III), probably by Cu reductase (*e.g.,* FRO4/5) before uptake by COPT1 [74, 79, 80].

For Cu(II) detoxification, glutathione or histidine-like ligands produced in plants bind with the absorbed Cu(II) by reduction or complexation, respectively. The subsequently formed Cu-organic complex, especially Cu(I)-glutathione, may translocate to the aerial part through the transpiration stream. Nevertheless, the detailed mechanism relating controlling transporters and genes for the uptake and reduction process of Cu by plant species merits further elucidation.

Implications for phytostabilization of contaminated areas

Our results indicated that the indigenous plant species grew well and adapted to mine contaminated soils with high concentrations of heavy metals and poor nutrient conditions. This study showed that the rhizosphere niche facilitates the availability of P and nitrogen nutrients, probably by plant root exudates or through microbial metabolism [81, 82]. On the other hand, organic exudates, including amino acids and organic acids, also favour the acquisition and subsequent immobilization of available trace metals from the soil to plants [10, 34, 83].

The concentrations of Cu and other trace metals such as Zn and Pb in the shoots

from the collected plants pose a low health risk to wild organisms, because the trace metals are lower than the US domestic animal toxicity limits for cattle [70]. The absorbed heavy metals are largely sequestered by complexing with alginate structures in the plant root; therefore, the contaminated mine soils can be physically stabilized under plant culture, showing the potential of ecological restoration. Coupling to the relatively high amount of nutrients, including P and N, in the rhizosphere, *M. floridulus* may be used for *in situ* phytostabilization of heavy metals in the mining area, which also limits the transportation of metal contaminants to the food chain [9, 33].

Acknowledgements

The work was supported by the National Natural Science Foundation of China (41603093), the National Basic Research Program of China (973 Program, 2014CB441101), and the RGC Collaborative Research Fund (RGC C7044-14G). We acknowledge Prof. Wen-sheng Shu and Dr. Bin Liao for advice on the field sampling work. We thank Dr. Ke-jian Peng for identifying the plant species. Copper(I)-cysteine XAS data was kindly provided by the group of Prof. Jian-jun Yang, Li-juan Sun, and Ji-yan Shi. The μ-XRF and μ-XANES results were acquired at beamline 15U at SSRF, and other XANES were collected at beamlines 01C1 and 16A1 at the National Synchrotron Radiation Research Center (NSRRC) in Taiwan.

References

[1] Z. Y. Li, Z. W. Ma, T. J. van der Kuijp, Z. W. Yuan, L. Huang, A review of soil heavy metal pollution from mines in China: Pollution and health risk assessment, Science of the Total Environment 468 (2014) 843-853.

[2] J. M. Zhou, Z. Dang, M. F. Cai, C. Q. Liu, Soil heavy metal pollution around the Dabaoshan Mine, Guangdong Province, China, Pedosphere 17 (2007) 588-594.

[3] P. Zhuang, M. B. McBride, H. Xia, N. Li, Z. Li, Health risk from heavy metals via consumption of food crops in the vicinity of Dabaoshan mine, South China, Science of The Total Environment 407 (2009) 1551-1561.

[4] J. L. Cui, Y. P. Zhao, Y. J. Lu, T. S. Chan, L. L. Zhang, D. C. W. Tsang, X. D. Li, Distribution and speciation of copper in rice (Oryza sativa L.) from mining-impacted paddy soil: Implications for copper uptake mechanisms, Environment International 126 (2019) 717-726.

[5] H. Ali, E. Khan, M. A. Sajad, Phytoremediation of heavy metals-Concepts and applications,

Chemosphere 91 (2013) 869-881.
[6] D. M. Poncelet, N. Cavender, T. J. Cutright, J. M. Senko, An assessment of microbial communities associated with surface mining-disturbed overburden, Environmental Monitoring and Assessment 186 (2014) 1917-1929.
[7] L. Wang, K. Yu, J.-S. Li, D. C. W. Tsang, C. S. Poon, J.-C. Yoo, K. Baek, S. Ding, D. Hou, J.-G. Dai, Low-carbon and low-alkalinity stabilization/solidification of high-Pb contaminated soil, Chemical Engineering Journal 351 (2018) 418-427.
[8] S. X. Yang, B. Liao, Z. H. Yang, L. Y. Chai, J. T. Li, Revegetation of extremely acid mine soils based on aided phytostabilization: A case study from southern China, Science of The Total Environment 562 (2016) 427-434.
[9] M. H. Wong, Ecological restoration of mine degraded soils, with emphasis on metal contaminated soils, Chemosphere 50 (2003) 775-780.
[10] F. D. Dakora, D. A. Phillips, Root exudates as mediators of mineral acquisition in low-nutrient environments, Plant and Soil 245 (2002) 35-47.
[11] C. L. Luo, Z. G. Shen, X. D. Li, Enhanced phytoextraction of Cu, Pb, Zn and Cd with EDTA and EDDS, Chemosphere 59 (2005) 1-11.
[12] D. Leštan, C. L. Luo, X. D. Li, The use of chelating agents in the remediation of metal-contaminated soils: A review, Environmental Pollution 153 (2008) 3-13.
[13] Y. P. Zhao, J. L. Cui, T. S. Chan, J. C. Dong, D. L. Chen, X. D. Li, Role of chelant on Cu distribution and speciation in Lolium multiflorum by synchrotron techniques, Science of The Total Environment 621 (2018) 772-781.
[14] H. Kupper, B. Gotz, A. Mijovilovich, F. C. Kupper, W. Meyer-Klaucke, Complexation and toxicity of copper in higher plants. I. Characterization of copper accumulation, speciation, and toxicity in Crassula helmsii as a new copper accumulator, Plant Physiology 151 (2009) 702-714.
[15] A. Mijovilovich, B. Leitenmaier, W. Meyer-Klaucke, P. M. H. Kroneck, B. Gotz, H. Kupper, Complexation and toxicity of copper in higher plants. II. Different mechanisms for copper versus cadmium detoxification in the copper-sensitive cadmium/zinc hyperaccumulator Thlaspi caerulescens (Ganges Ecotype), Plant Physiology 151 (2009) 715-731.
[16] B. Collin, E. Doelsch, C. Keller, P. Cazevieille, M. Tella, P. Chaurand, F. Panfili, J.-L. Hazemann, J.-D. Meunier, Evidence of sulfur-bound reduced copper in bamboo exposed to high silicon and copper concentrations, Environmental Pollution 187 (2014) 22-30.
[17] D. Jouvin, D. J. Weiss, T. F. M. Mason, M. N. Bravin, P. Louvat, F. Zhao, F. Ferec, P. Hinsinger, M. F. Benedetti, Stable isotopes of Cu and Zn in higher plants: Evidence for Cu reduction at the root surface and two conceptual models for isotopic fractionation processes, Environmental Science & Technology 46 (2012) 2652-2660.
[18] B. M. Ryan, J. K. Kirby, F. Degryse, H. Harris, M. J. McLaughlin, K. Scheiderich, Copper speciation and isotopic fractionation in plants: uptake and translocation mechanisms, New Phytologist 199 (2013) 367-378.
[19] L. L. Lu, R. H. Xie, T. Liu, H. X. Wang, D. D. Hou, Y. H. Du, Z. L. He, X. E. Yang, H. Sun, S. K. Tian, Spatial imaging and speciation of Cu in rice (Oryza sativa L.) roots using synchrotron-based X-ray microfluorescence and X-ray absorption spectroscopy, Chemosphere 175 (2017) 356-364.
[20] S. Chen, J. Chen, L. Xie, J. Liao, J. Zhang, Q. Yang, Heavy metal accumulation characteristics of plants in Dabaoshan mine in Guangdong Province, Journal of

soil and water conservation (In Chinese) 6 (2011) 216-220.
[21] J. Qin, B. Xia, M. Hu, P. Zhao, H. Zhao, X. Lin, Analysis of the vegetation succession of tailing wasterland of Dabaoshan mine, Guangdong Province, Journal of Agro-Environment Science (In Chinese) 28 (2009) 1-7.
[22] X. F. Hu, F. S. Chen, M. L. Wine, X. M. Fang, Increasing acidity of rain in subtropical tea plantation alters aluminum and nutrient distributions at the root-soil interface and in plant tissues, Plant and Soil 417 (2017) 261-274.
[23] M. R. Carter, E. G. Gregorich, Soil sampling and methods of analysis. CRC Press: 2006.
[24] X. D. Li, S. L. Lee, S. C. Wong, W. Z. Shi, L. Thornton, The study of metal contamination in urban soils of Hong Kong using a GIS-based approach, Environmental Pollution 129 (2004) 113-124.
[25] L. Krajcarová, K. Novotný, M. Kummerová, J. Dubová, V. Gloser, J. Kaiser, Mapping of the spatial distribution of silver nanoparticles in root tissues of Vicia faba by laser-induced breakdown spectroscopy (LIBS), Talanta 173 (2017) 28-35.
[26] J. L. Cui, J. B. Shi, G. B. Jiang, C. Y. Jing, Arsenic levels and speciation from ingestion exposures to biomarkers in Shanxi, China: Implications for human health, Environmental Science & Technology 47 (2013) 5419-5424.
[27] L. L. Zhang, S. Yan, S. Jiang, K. Yang, H. Wang, S. M. He, D. X. Liang, L. Zhang, Y. He, X. Y. Lan, C. W. Mao, J. Wang, H. Jiang, Y. Zheng, Z. H. Dong, L. Y. Zeng, A. G. Li, Hard X-ray micro-focusing beamline at SSRF, Nuclear Science and Techniques 26 (2015).
[28] S. Wei, Q. Zhou, S. Mathews, A newly found cadmium accumulator-Taraxacum mongolicum, Journal of Hazardous Materials 159 (2008) 544-547.
[29] S. M. Webb, SIXpack: a graphical user interface for XAS analysis using IFEFFIT, Phys. Scr. T115 (2005) 1011-1014.
[30] A. Manceau, M. A. Marcus, N. Tamura, Quantitative speciation of heavy metals in soils and sediments by synchrotron X-ray techniques, Rev. Mineral. Geochemistry 49 (2002) 341-428.
[31] B. Ravel, M. Newville, ATHENA, ARTEMIS, HEPHAESTUS: data analysis for X-ray absorption spectroscopy using IFEFFIT, Journal of Synchrotron Radiation 12 (2005) 537-541.
[32] J. L. Cui, C. Y. Jing, D. S. Che, J. F. Zhang, S. X. Duan, Groundwater arsenic removal by coagulation using ferric(III) sulfate and polyferric sulfate: A comparative and mechanistic study, Journal of Environmental Sciences 32 (2015) 42-53.
[33] A. Pérez-de-Mora, E. Madejón, P. Burgos, F. Cabrera, Trace element availability and plant growth in a mine-spill-contaminated soil under assisted natural remediation: II. Plants, Science of The Total Environment 363 (2006) 38-45.
[34] C. Kaur, G. Selvakumar, A. N. Ganeshamurthy, Organic acids in the rhizosphere: Their role in phosphate dissolution. In Microbial Inoculants in Sustainable Agricultural Productivity Vol. 2: Functional Applications, Singh, D. P.; Singh, H. B.; Prabha, R., Eds. Springer India: New Delhi, 2016; pp 165-177.
[35] J. L. Cui, Y. P. Zhao, J. S. Li, J. Z. Beiyuan, D. C. W. Tsang, C. S. Poon, T. S. Chan, W. X. Wang, X. D. Li, Speciation, mobilization, and bioaccessibility of arsenic in geogenic soil profile from Hong Kong, Environmental Pollution 232 (2018) 375-384.
[36] J. Zhang, S. Y. Yang, Y. J. Huang, S. B. Zhou, The tolerance and accumulation of *Miscanthus Sacchariflorus* (maxim.) Benth., an energy plant species, to cadmium, International Journal of Phytoremediation 17 (2015) 538-545.

[37] N. S. Bolan, J. H. Park, B. Robinson, R. Naidu, K. Y. Huh, Chapter four - Phytostabilization: A Green Approach to Contaminant Containment. In Advances in Agronomy, Sparks, D. L., Ed. Academic Press: 2011; Vol. 112, pp 145-204.

[38] V. de la Fuente, L. Rufo, N. Rodríguez, A. Franco, R. Amils, Comparison of iron localization in wild plants and hydroponic cultures of Imperata cylindrica (L.) P. Beauv, Plant and Soil 418 (2017) 25-35.

[39] H. Feng, Y. Qian, F. J. Gallagher, W. G. Zhang, L. Z. Yu, C. J. Liu, K. W. Jones, R. Tappero, Synchrotron micro-scale measurement of metal distributions in Phragmites australis and Typha latifolia root tissue from an urban brownfield site, Journal of Environmental Sciences 41 (2016) 172-182.

[40] L. V. Kochian, M. A. Piñeros, J. Liu, J. V. Magalhaes, Plant adaptation to acid soils: The molecular basis for crop aluminum resistance, Annual Review of Plant Biology 66 (2015) 571-598.

[41] T. Haruma, K. Yamaji, H. Masuya, K. Hanyu, Root endophytic Chaetomium cupreum promotes plant growth and detoxifies aluminum in Miscanthus sinensis Andersson growing at the acidic mine site, Plant Species Biology 33 (2018) 109-122.

[42] Y. Ye, D. Chunyan, G. Lanping, Q. Yuan, Y. Xiaoyan, C. Qi, L. Diqiu, W. Chengxiao, C. Xiuming, Distribution pattern of aluminum in Panax notoginseng, a native medicinal plant adapted to acidic red soils, Plant and Soil 423 (2018) 375-384.

[43] J. F. Ma, P. R. Ryan, E. Delhaize, Aluminium tolerance in plants and the complexing role of organic acids, Trends in Plant Science 6 (2001) 273-278.

[44] E. Olivares, E. Peña, E. Marcano, J. Mostacero, G. Aguiar, M. Benítez, E. Rengifo, Aluminum accumulation and its relationship with mineral plant nutrients in 12 pteridophytes from Venezuela, Environmental and Experimental Botany 65 (2009) 132-141.

[45] G. Sarret, E. Smits, H. C. Michel, M. P. Isaure, F. J. Zhao, R. Tappero, Use of synchrotron-based techniques to elucidate metal uptake and metabolism in plants, Advances in Agronomy 119 (2013) 1-82.

[46] A. Chabbi, Metal concentrations in pore water of the Lusatian lignite mining sediments and internal metal distribution in Juncus bulbosus, Water, Air and Soil Pollution: Focus 3 (2003) 105-117.

[47] A.-M. Aucour, J.-P. Bedell, M. Queyron, R. Thole, A. Lamboux, G. Sarret, Zn speciation and stable isotope fractionation in a contaminated urban wetland soil-Typha latifolia system, Environmental Science & Technology 51 (2017) 8350-8358.

[48] T. Fresno, J. M. Peñalosa, J. Santner, M. Puschenreiter, T. Prohaska, E. Moreno-Jiménez, Iron plaque formed under aerobic conditions efficiently immobilizes arsenic in Lupinus albus L roots, Environmental Pollution 216 (2016) 215-222.

[49] L. J. Furnare, A. Vailionis, D. G. Strawn, Polarized XANES and EXAFS spectroscopic investigation into copper(II) complexes on vermiculite, Geochimica et Cosmochimica Acta 69 (2005) 5219-5231.

[50] L. S. Kau, D. J. Spira-Solomon, J. E. Penner-Hahn, K. O. Hodgson, E. I. Solomon, X-ray absorption edge determination of the oxidation state and coordination number of copper. Application to the type 3 site in Rhus vernicifera laccase and its reaction with oxygen, Journal of the American Chemical Society 109 (1987) 6433-6442.

[51] D. G. Strawn, L. L. Baker, Speciation of Cu in a contaminated agricultural soil measured by XAFS, μ-XAFS, and μ-XRF, Environmental Science & Technology 42 (2008) 37-42.

[52] M. T. Nielsen, J. J. Scott-Fordsmand, M. W. Murphy, S. M. Kristiansen, Speciation and solubility

of copper along a soil contamination gradient, Journal of Soils and Sediments 15 (2015) 1558-1570.
[53] L. Guo, T. J. Cutright, Effect of citric acid and bacteria on metal uptake in reeds grown in a synthetic acid mine drainage solution, Journal of Environmental Management 150 (2015) 235-242.
[54] M. F. Dong, R. W. Feng, R. G. Wang, Y. Sun, Y. Z. Ding, Y. M. Xu, Z. L. Fan, J. K. Guo, Inoculation of Fe/Mn-oxidizing bacteria enhances Fe/Mn plaque formation and reduces Cd and As accumulation in Rice Plant tissues, Plant and Soil 404 (2016) 75-83.
[55] Z. H. Ye, A. J. M. Baker, M. H. Wong, A. J. Willis, Zinc, lead and cadmium accumulation and tolerance in Typha latifolia as affected by iron plaque on the root surface, Aquatic Botany 61 (1998) 55-67.
[56] J. Yang, G. Zheng, J. Yang, X. Wan, B. Song, W. Cai, J. Guo, Phytoaccumulation of heavy metals (Pb, Zn, and Cd) by 10 wetland plant species under different hydrological regimes, Ecological Engineering 107 (2017) 56-64.
[57] C. M. Hansel, S. Fendorf, S. Sutton, M. Newville, Characterization of Fe plaque and associated metals on the roots of mine-waste impacted aquatic plants, Environmental Science & Technology 35 (2001) 3863-3868.
[58] W. J. Liu, Y. G. Zhu, Y. Hu, P. N. Williams, A. G. Gault, A. A. Meharg, J. M. Charnock, F. A. Smith, Arsenic sequestration in iron plaque, its accumulation and speciation in mature rice plants (Oryza Sativa L.), Environmental Science & Technology 40 (2006) 5730-5736.
[59] W. C. Li, H. Deng, M. H. Wong, Effects of Fe plaque and organic acids on metal uptake by wetland plants under drained and waterlogged conditions, Environmental Pollution 231 (2017) 732-741.
[60] J. J. Yang, J. Liu, J. J. Dynes, D. Peak, T. Regier, J. Wang, S. H. Zhu, J. Y. Shi, J. S. Tse, Speciation and distribution of copper in a mining soil using multiple synchrotron-based bulk and microscopic techniques, Environmental Science and Pollution Research 21 (2014) 2943-2954.
[61] M. Krzesłowska, The cell wall in plant cell response to trace metals: polysaccharide remodeling and its role in defense strategy, Acta Physiologiae Plantarum 33 (2011) 35-51.
[62] M. Adrees, S. Ali, M. Rizwan, M. Ibrahim, F. Abbas, M. Farid, M. Zia-ur-Rehman, M. K. Irshad, S. A. Bharwana, The effect of excess copper on growth and physiology of important food crops: a review, Environmental Science and Pollution Research 22 (2015) 8148-8162.
[63] P. Wang, N. W. Menzies, E. Lombi, B. A. McKenna, M. D. de Jonge, E. Donner, F. P. C. Blamey, C. G. Ryan, D. J. Paterson, D. L. Howard, S. A. James, P. M. Kopittke, Quantitative determination of metal and metalloid spatial distribution in hydrated and fresh roots of cowpea using synchrotron-based X-ray fluorescence microscopy, Science of The Total Environment 463-464 (2013) 131-139.
[64] A. Probst, H. Y. Liu, M. Fanjul, B. Liao, E. Hollande, Response of Vicia faba L. to metal toxicity on mine tailing substrate: Geochemical and morphological changes in leaf and root, Environmental and Experimental Botany 66 (2009) 297-308.
[65] A. Sofo, R. Bochicchio, M. Amato, N. Rendina, A. Vitti, M. Nuzzaci, M. M. Altamura, G. Falasca, F. D. Rovere, A. Scopa, Plant architecture, auxin homeostasis and phenol content in Arabidopsis thaliana grown in cadmium- and zinc-enriched media, Journal of Plant Physiology 216 (2017) 174-180.
[66] J. Y. Shi, X. F. Yuan, X. C. Chen, B. Wu, Y. Y. Huang, Y. X. Chen, Copper uptake and its effect on metal distribution in root growth zones of Commelina communis revealed by SRXRF, Biological Trace Element Research 141 (2011) 294-304.

[67] J. L. Hall, Cellular mechanisms for heavy metal detoxification and tolerance, Journal of Experimental Botany 53 (2002) 1-11.
[68] A. Manceau, A. Simionovici, M. Lanson, J. Perrin, R. Tucoulou, S. Bohic, S. C. Fakra, M. A. Marcus, J.-P. Bedell, K. L. Nagy, Thlaspi arvense binds Cu(II) as a bis-(l-histidinato) complex on root cell walls in an urban ecosystem, Metallomics 5 (2013) 1674-1684.
[69] C. Jeon, J. Y. Park, Y. J. Yoo, Characteristics of metal removal using carboxylated alginic acid, Water Research 36 (2002) 1814-1824.
[70] E. Fourest, B. Volesky, Contribution of sulfonate groups and alginate to heavy metal biosorption by the dry biomass of Sargassum fluitans, Environmental Science & Technology 30 (1996) 277-282.
[71] A. J. M. Baker, Accumulators and excluders - strategies in the response of plants to heavy metals, Journal of Plant Nutrition 3 (1981) 643-654.
[72] L. A. Polette, J. L. Gardea-Torresdey, R. R. Chianelli, G. N. George, I. J. Pickering, J. Arenas, XAS and microscopy studies of the uptake and bio-transformation of copper in Larrea tridentata (creosote bush), Microchemical Journal 65 (2000) 227-236.
[73] B. Irtelli, W. A. Petrucci, F. Navari-Izzo, Nicotianamine and histidine/proline are, respectively, the most important copper chelators in xylem sap of Brassica carinata under conditions of copper deficiency and excess, Journal of Experimental Botany 60 (2009) 269-277.
[74] B. Printz, S. Lutts, J. F. Hausman, K. Sergeants, Copper trafficking in plants and its implication on cell wall dynamics, Frontiers in Plant Science 7 (2016).
[75] C. M. Palmer, M. L. Guerinot, Facing the challenges of Cu, Fe and Zn homeostasis in plants, Nature Chemical Biology 5 (2009) 333-340.
[76] R. Araki, J. Murata, Y. Murata, A novel barley yellow stripe 1-like transporter (HvYSL2) localized to the root endodermis transports metal-phytosiderophore complexes, Plant and Cell Physiology 52 (2011) 1931-1940.
[77] C. Curie, G. Cassin, D. Couch, F. Divol, K. Higuchi, M. Jean, J. Misson, A. Schikora, P. Czernic, S. Mari, Metal movement within the plant: contribution of nicotianamine and yellow stripe 1-like transporters, Annals of Botany 103 (2009) 1-11.
[78] C. Peng, Y. Wang, L. J. Sun, C. Xu, L. J. Zhang, J. Y. Shi, Distribution and speciation of Cu in the root border cells of rice by STXM combined with NEXAFS, Bulletin of Environmental Contamination and Toxicology 96 (2016) 408-414.
[79] M. Yuan, X. H. Li, J. H. Xiao, S. P. Wang, Molecular and functional analyses of COPT/Ctr-type copper transporter-like gene family in rice, Bmc Plant Biology 11 (2011).
[80] M. Bernal, D. Casero, V. Singh, G. T. Wilson, A. Grande, H. Yang, S. C. Dodani, M. Pellegrini, P. Huijser, E. L. Connolly, S. S. Merchant, U. Krämer, Transcriptome sequencing identifies SPL7-regulated copper acquisition genes FRO_4/FRO_5 and the copper dependence of iron homeostasis in *Arabidopsis*, The Plant Cell 24 (2012) 738-761.
[81] L. E. Jackson, M. Burger, T. R. Cavagnaro, Roots, nitrogen transformations, and ecosystem services, Annual Review of Plant Biology 59 (2008) 341-363.
[82] M. Burger, L. E. Jackson, Plant and microbial nitrogen use and turnover: Rapid conversion of nitrate to ammonium in soil with roots, Plant and Soil 266 (2005) 289-301.
[83] J. L. Cui, C. L. Luo, C. W. Y. Tang, T. S. Chan, X. D. Li, Speciation and leaching of trace metal contaminants from e-waste contaminated soils, Journal of Hazardous Materials 329 (2017) 150-158.

673 **List of Figures**

674 Figure 1. Light microscope and micro-X-ray fluorescence (μ-XRF) images around the
675 root cross-section of *M. floridulus.* The white box in the root graph (g) shows where μ-
676 XRF maps were obtained.

677

678 Figure 2. Copper K-edge XANES analysis for the standard references (I) and the
679 rhizosphere and non-rhizosphere soil (bulk-XANES) and the interested spots (IS 1-4,
680 μ-XANES) in the plant root thin section from Figure 1. The collected XANES data for
681 the samples are shown as black circles with linear combination fitting (LCF) as red
682 lines (II). The vertical lines are the pre-edge of Cu(I) characterized by Cu-glutathione.
683 The linear combination fitting results are shown in Table 3. The dashed vertical regions
684 represent the pre-edge of Cu(I)-glutathione/Cu(I)-cysteine (a) and Cu(II) (b),
685 respectively. Plant A and B represent *M. floridulus* and *S. chusana*, respectively, shown
686 in Table 1.

687

688 Figure 3. Iron K-edge XANES analysis for the standard references (I) and the soil
689 samples (II). The collected XANES data for the samples are shown as black circles with
690 linear combination fitting (LCF) as red lines (II). The linear combination fitting results
691 are shown in Table S3. Plant A and B represent *M. floridulus* and *S. chusana*,
692 respectively.

693

694 Figure 4. A conceptual model of possible uptake and transformation mechanism for Cu
695 *M. floridulus* plant based on the findings in this study coupling with previous studies
696 [75, 76, 79, 80]. Some abbreviations: Al for alginate, GSH for glutathione, Hi for
697 histidine, PS for phytosiderophore, YSL for yellow strip 1-like transporter, FRO4/5 for
698 Fe or Cu reductase, and COPT1 for Copper transporter protein.

699

700 **List of Tables**

701 Table 1. The pH of soil extracted using deionized water, and available TOC,
702 phosphorous (P), nitrate, ammonium, Cu, Fe, Al, and Mn in rhizosphere and non-

703 rhizosphere soil after $CaCl_2$ extraction (mg/L). The numbers in the bracket represent
704 the error bars of triplicate analysis.
705
706 Table 2. Concentrations of Cu (mg/kg), Fe (mg/kg), Al (mg/kg), and Mn (mg/kg) in the
707 rhizosphere soil (RS), non-rhizosphere soil (NRS), and plant samples and the
708 corresponding bioaccumulation factor (BCF) and translocation factor (TF).
709
710 Table 3. Copper species (%) in the mining soil and selected spots in the roots (Figure
711 1) using linear combination fit analysis of Cu K-edge XANES (Figure 2). Some Cu
712 standards were not detected (ND) during XANES analysis, and other Cu standards
713 (Figure 2-I) with no detection were not listed.
714

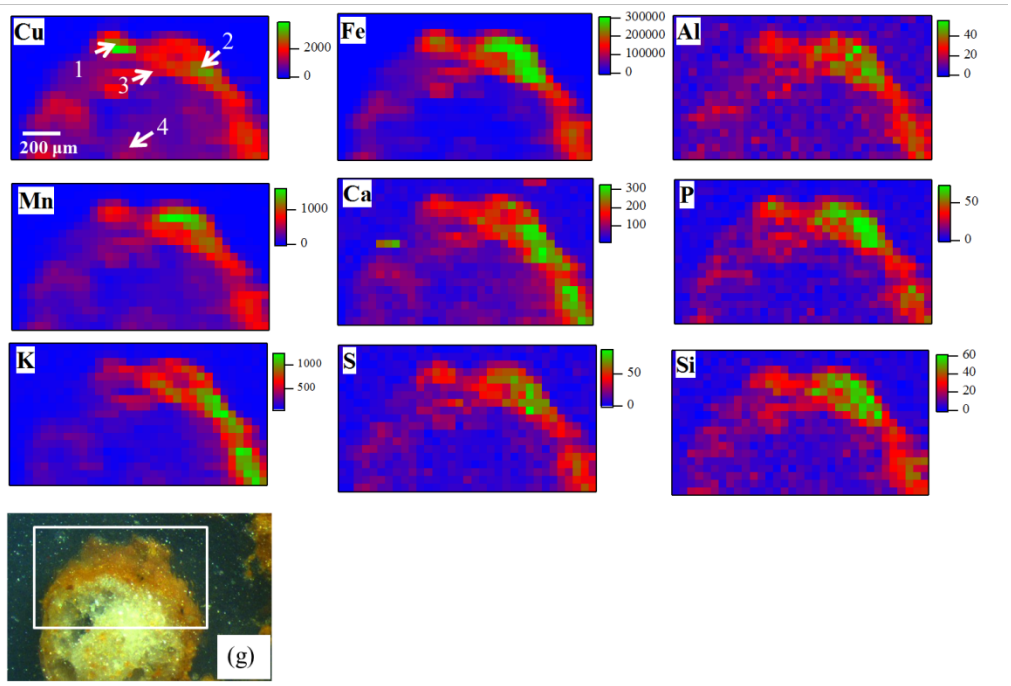
Cu
1
2
3
4
200 µm
2000
0
Fe
300000
200000
100000
0
Al
40
20
0
Mn
1000
0
Ca
300
200
100
P
50
0
K
1000
500
S
50
0
Si
60
40
20
0
(g)

Figure 1

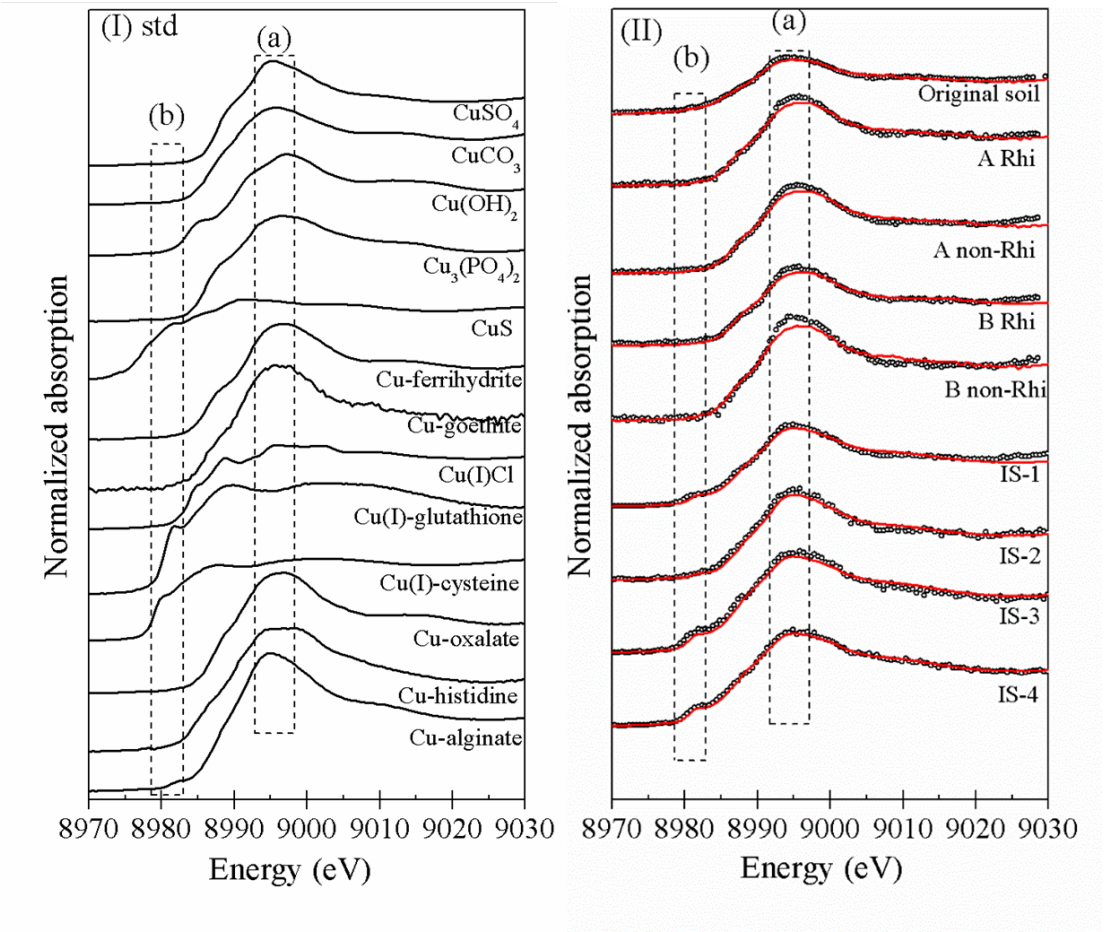

719

720 Figure 2

721

722

723

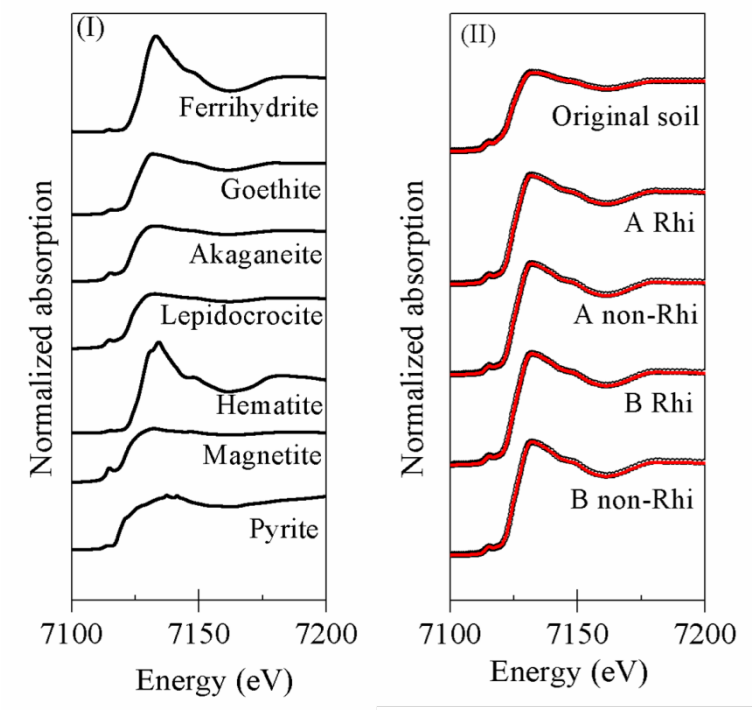

724

725 Figure 3

726

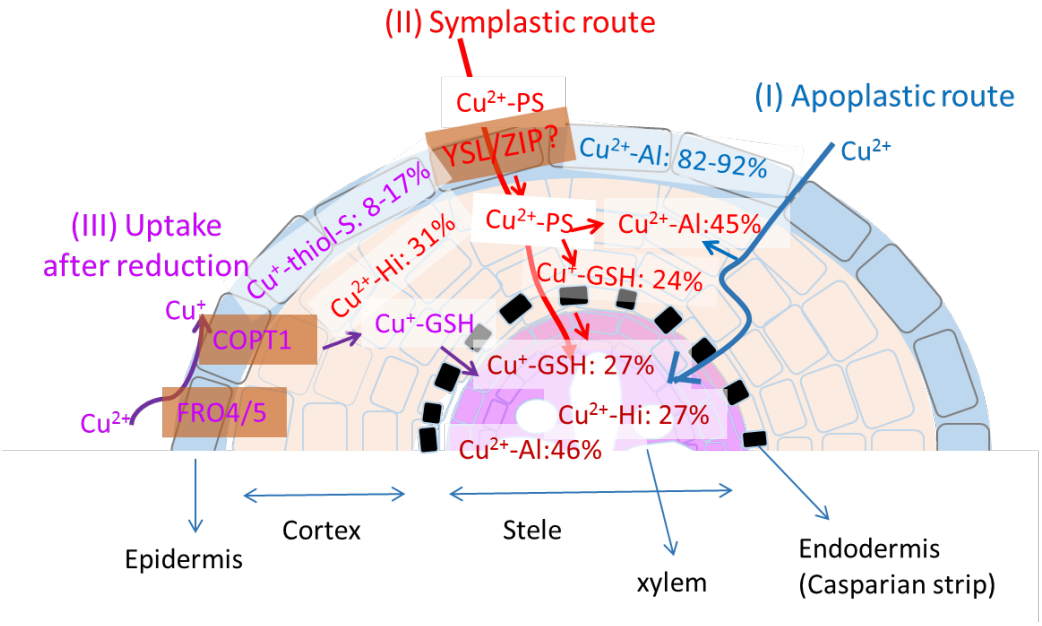
(II) Symplastic route
Cu2+-PS
(I) Apoplastic route
YSL/ZIP?
Cu2+-Al: 82-92%
Cu2+
(III) Uptake
after reduction
Cu+-thiol-S: 8-17%
Cu2+-PS
Cu2+-Al:45%
Cu2+-Hi: 31%
Cu+-GSH: 24%
Cu+
COPT1
Cu+-GSH
Cu+-GSH: 27%
Cu2+
FRO4/5
Cu2+-Hi: 27%
Cu2+-Al:46%
Epidermis
Cortex
Stele
xylem
Endodermis
(Casparian strip)

Figure 4

735 Table 1

	M. floridulus		*S. chusana*	
	Rhizosphere	Non-Rhizosphere	Rhizosphere	Non-Rhizosphere
pH	3.48(0.05)	3.52 (0.02)	4.38 (0.01)	4.56 (0.01)
TOC	9.2 (0.0)	5.0 (0.6)	12.6 (0.2)	4.8 (0.6)
P	0.18 (0.04)	0.14 (0.05)	0.20 (0.07)	0.16 (0.01)
Nitrate	5.2 (0.68)	1.06 (0.51)	2.51 (0.68)	0.30 (0.26)
Ammonia	0.16 (0.03)	0.01 (0.00)	0.06 (0.01)	0.05 (0.01)
Fe	0.21 (0.01)	0.11 (0.01)	0.01 (0.01)	0.01 (0.01)
Mn	0.50 (0.00)	1.34 (0.01)	2.17 (0.03)	0.28 (0.02)
Al	4.14 (0.46)	9.88 (0.07)	4.72 (0.65)	2.04 (0.67)
Cu	1.34 (0.06)	1.02 (0.03)	0.08 (0.00)	0.06 (0.03)

736

Table 2

Sample		Cu	Fe	Al	Mn
Soil	Original mine soil	3150	316000	109000	5690
Soil	*M. floridulus* RS	922	170000	109000	450
Soil	*M. floridulus* NRS	1050	199000	106000	550
Soil	*S. chusana* RS	1170	210000	108000	1120
Soil	*S. chusana* NRS	752	168000	109000	820
Plant root	*M. floridulus*	264	2850	870	0.5
Plant root	*S. chusana*	535	8050	8000	2.5
Plant shoot	*M. floridulus*	29.4	498	203	2.6
Plant shoot	*S. chusana*	19.6	204	357	11.7
BCF	*M. floridulus*	0.29	0.02	0.01	0.00
BCF	*S. chusana*	0.46	0.04	0.07	0.00
TF	*M. floridulus*	0.11	0.17	0.23	5.20
TF	*S. chusana*	0.04	0.03	0.04	4.68

Table 3

Sample	Cu-Gt	CuS	Cu-oxalate	Cu-alginate	Cu(I)-glutathione	Cu(I)-	Cu-	R-Factor	χ^2
Original mining soil	72	12	16	ND	ND	ND	ND	0.0017	0.0010
M. floridulus Rhi	54	ND	46	ND	ND	ND	ND	0.0028	0.0018
M. floridulus non-Rhi	45	ND	55	ND	ND	ND	ND	0.0028	0.0018
S. chusana Rhi	20	ND	80	ND	ND	ND	ND	0.0025	0.0013
S. chusana non-Rhi	69	ND	31	ND	ND	ND	ND	0.0057	0.0046
IS-1				82	5	12	ND	0.0141	0.2662
IS-2				92	ND	8	ND	0.0059	0.1234
IS-3				45	31	ND	31	0.0274	0.6122
IS-4				46	27	ND	27	0.0085	0.1560

R factor, goodness-of-fit parameter, $\Sigma(\chi_{data} - \chi_{fit})^2/\Sigma(\chi_{data})^2$; χ^2 represents the fitting quality of the XANES data.